ELSEVIER

Journal of Nuclear Materials 290–293 (2001) 920–924

journal of nuclear materials

www.elsevier.nl/locate/jnucmat

On the way to divertor detachment in the W7-AS stellarator

K. McCormick *, P. Grigull, R. König, R. Burhenn, H. Ehmler, Y. Feng, S. Fiedler, L. Giannone, D. Hildebrandt, J.P. Knauer, G. Kühner, D. Naujoks, J. Sallander, Ch. Wendland, W7-AS Team

Max-Planck-Institut für Plasmaphysik, EURATOM-Association, Boltzmannstrasse 2, 85748 Garching, Germany

Abstract

3D modeling on W7-AS suggests that to obtain divertor plasma detachment, upstream separatrix densities n_{es} in the range of 10^{20} m^{-3} will be necessary. This paper investigates the ratio of n_{es} to the line-averaged density $\bar{n}_e$ under a variety of conditions – $P_{heat} \sim 0.4$–2 MW, $\bar{n}_e \sim 0.2$–2.7×10^{20} m^{-3} – for inner-limiter plasma configurations in preparation for the upcoming divertor phase. $n_{es}/\bar{n}_e$ ranges from 0.05 for the quiescent H-mode H^* ($P_{ecrh} \sim 0.4$ MW) up to $\sim$0.35 for high-power ($P_{nbi} \sim 2$ MW), heavily fueled discharges where n_{es} approaches 10^{20} m^{-3} within a density ramp. For $P_{nbi} < 1$ MW, $n_{es}/\bar{n}_e$ declines with increasing $\bar{n}_e$ as the H-mode threshold density $\bar{n}_e^{thr}$ approaches. L–H–L switching transitions cause $n_{es}/\bar{n}_e$ to alternate between higher and lower values. The attainment of H^* implies reduced $n_{es}/\bar{n}_e$ and incipient radiation collapse of the core plasma. $\bar{n}_e^{thr}$ and $n_{es}/\bar{n}_e$ both increase with heating power by which means detachment-relevant n_{es} can be attained, albeit at $\bar{n}_e$ close to the density limit. These phenomena in detail exhibit a sensitive dependence on ι_a – even a 1% change results in evident and reproducible plasma behavior.

Keywords: Plasma edge; SOL; W7-AS; Stellarator

1. Introduction

An essential feature of a fusion-reactor device is the capability of plasma-facing components to handle the associated power and particle fluxes. Whereas progress on tokamaks has been substantial, with the solution relying on at least a partially detached divertor plasma, investigations on stellarators to this end are in their infancy. The concept of a boundary–island divertor, native to the Wendelstein stellarator research line, will be implemented for the first time anywhere beginning in the summer of 2000. In preparation for this phase, preliminary studies of the relevant plasma configurations and edge parameters have been carried out with inboard sector limiters [1–5].

This article emphasizes the systematic dependence of the separatrix density n_{es} on line-averaged density $\bar{n}_e$ and heating power. First-approach 3D edge code calculations (EMC3) provide estimates of conditions necessary to achieve detachment: (1) $n_{es} \sim 2 \times 10^{20}$ m^{-3} is required – assuming impurities radiate such that a remaining 200 kW needs to be dissipated by the hydrogen plasma in the divertor and SOL [6]. (2) Including carbon sputtering ($\eta = 1.5\%$) in a self-consistent manner and a power flow $P_{sol} = 1$ MW into the SOL, yields the prediction $n_{es} \sim 8 \times 10^{19}$ m^{-3} [7]. The extent to which such densities can be attained depends on $n_{es}/\bar{n}_e$ and the density limit $\bar{n}_e^{DL}$. Multi-machine investigations (with $\iota_a \sim 0.34$, $B_t = 0.8$–2.5 T, $P_{heat} = 0.5$–2 MW for W7-AS) find that the stellarator experience can be summarized as $\bar{n}_e^{DL}$ $(10^{19}\ \mathrm{m}^{-3}) = 14.6[P_{abs}\ (\mathrm{MW})/V_p\ (\mathrm{m}^3)]^{0.48} B_t\ (\mathrm{T})^{0.54}$ [8]. This is the point where the plasma core suffers a (non-disruptive) radiation collapse – a region to avoid, as the goal is to achieve detachment through radiation in the divertor, not the main plasma.

Section 2 details edge/SOL/limiter plasma studies with heating powers $P_{heat} \sim 0.4$–2 MW and maximum attainable $\bar{n}_e$. Key diagnostics [9] upstream in the vicinity of the separatrix bordering the main plasma are: (a) single time-point Thomson scattering for $n_e(r)$, $T_e(r)$ [10],

* Corresponding author. Tel.: +49-089 3299 1932; fax: +49-089 3299 1932.

E-mail address: gkm@ipp.mpg.de (K. McCormick).

0022-3115/01/$ - see front matter
PII: S0022-3115(00)00472-4

(b) a single-stroke scannable Langmuir probe (RCP) for $n_e(r)$ and $T_e(r)$ in the SOL up to the separatrix, and (c) a high-energy Li beam for $n_e(r,t)$ -profiles. W7-AS consists of five modules, each of which has an upper and lower limiter, toroidally separated [1]. At the limiters: (a) an IR camera determines the 2D heat flux [11] (module 1), (b) 2D particle fluxes are monitored via an H_α-CCD camera (module 5) [5,12], and (c) arrays of flush-mounted Langmuir probes imbedded in two limiters (upper and lower of module 2) give $I_{sat}(t)$, $T_e(t)$ and $n_e(t)$.

2. Results and discussion

The following four experimental sets are studied:

1. $P_{nbi} \sim 0.4$ MW with ramped $\bar{n}_e$, highlighting differences in edge–core plasma behavior for $\iota_a \sim 0.558$ and 0.553,
2. $P_{ecrh} \sim 0.4$ and 0.8 MW for stationary-$\bar{n}_e$ and ramps at $\iota_a \sim 0.564$,
3. $P_{ecrh} \sim 0.4$ MW and $P_{nbi} \sim 0.4$–1.2 MW at $\iota_a \sim 0.558$ with $\bar{n}_e$-ramps, and
4. $P_{nbi} \sim 2$ MW in fast $\bar{n}_e$-ramps to maximize n_{es} at $\iota_a \sim 0.561$.

2.1. Sensitivity to ι_a

Fig. 1 depicts the temporal evolution of two NBI-heated discharges differing by $\delta\iota_a \sim 0.005$. They digress in that $\iota_a = 0.558$ exhibits a transition into the quiescent H-mode H^* at ~0.37 s with a concomitant increase in plasma energy W_{dia}, which then rolls over as the total plasma radiation P_{rad} approaches P_{abs}. Power and particle fluxes into the SOL decrease abruptly at the H^*-transition, evidenced by the drops in T_e^{lim} and in saturation current I_{sat}^{lim} to a limiter probe as well as H_α intensity at a limiter. The density profile e-folding length λ_{in} (measured in Li-beam coordinates) inside the separatrix also steepens dramatically (corroborated on other discharges with the edge Thomson system [10]), with little change in λ_{out} outside the separatrix. In this case, n_{es} also decreases by ~30%. Nonetheless, these phenomena are largely transient, with many edge-related traces (n_{es}, T_e^{lim}, H_α) reconverging before W_{dia} has peaked. Of particular interest, in addition to the effects which minor changes in ι_a can evoke, is the conduct of $n_{es}/\bar{n}_e$ with density. The increase from $n_{es}/\bar{n}_e \sim 0.13$ to 0.17 over 0.21–0.26 s can be attributed to the augmented gas puff used to initiate the density ramp. The subsequent decrease from ~0.17 to 0.1 as the density ramp proceeds is typical for low-power discharges. It is correlated with the observed decline in transport coefficients with higher densities of which here W_{dia} and λ_{in} are indicators. In any case, the n_{es} values attained are far from those needed for detachment or even for high recycling at the limiter/divertor.

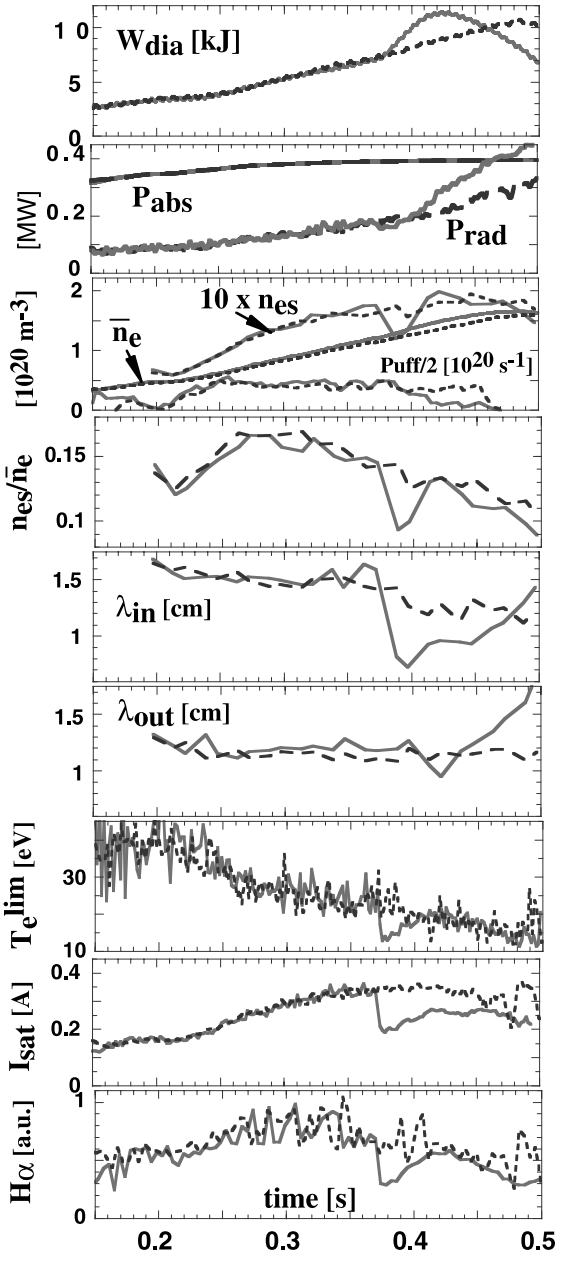

Fig. 1. Temporal evolution of global and edge parameters for two NBI-heated discharges: $\iota_a = 0.553$ (dashed line, #45268); $\iota_a = 0.558$ (solid, #45265); $B_t = 2.5$ T.

2.2. Behavior at $P_{ecrh} = 0.4$ and 0.8 MW

ECRH discharges have the advantage of density control, allowing steady-state conditions. Unfortunately, they are limited by the 140 GHz cut-off density of 1.2×10^{20} m^{-3}. Fig. 2 shows $n_{es}/\bar{n}_e$ vs. for two power levels $P_{ecrh} \sim 0.4/0.8$ MW, maintained over 1/0.7 s for a

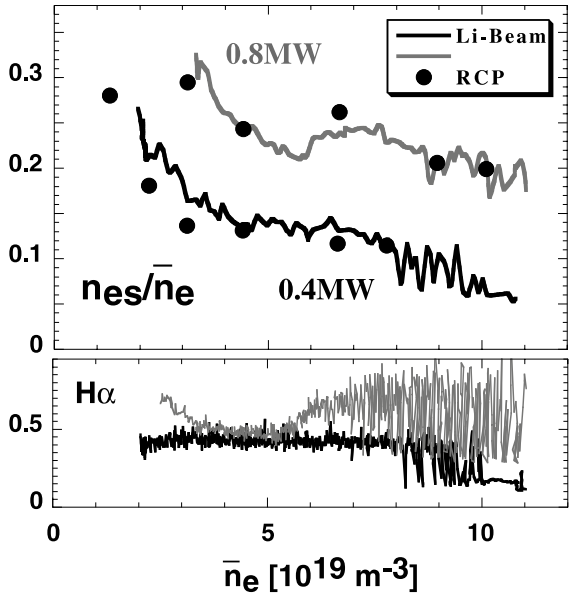

Fig. 2. Ratio of n_{es} to $\bar{n}_e$ vs. $\bar{n}_e$ for two sets of discharges at $\iota_a = 0.564$ for $P_{ecrh} \sim 0.4/0.8$ MW: solid lines – Li-beam values during $\bar{n}_e$-ramps (#46333 and #46337); points – RCP measurements during steady-state discharges; bottom – H_α at a limiter for #46333, #46337 (top trace).

series of density plateaus and two encompassing density ramps. Results from the RCP are for the steady-state cases, whereby the separatrix was taken to be that point where the floating potential reached −50 V. This information was used to calibrate the separatrix position for the Li beam. (The Li values are nearer those of RCP when taken for the flat-top cases – not shown.) At 0.4 MW $n_{es}/\bar{n}_e$ varies as ~0.25–>0.12 over $\bar{n}_e \sim 2$–$> 8 \times 10^{19}$ m^{-3}, whereupon an H-mode transition occurs first in a dithering fashion causing $n_{es}/\bar{n}_e$ to oscillate between ~ 0.12–0.07, followed by H^* and $n_{es}/\bar{n}_e \sim 0.06$. At 0.8 MW $n_{es}/\bar{n}_e$ assumes values about twice those at 0.4 MW, also decreases with higher $\bar{n}_e$ and also undergoes small oscillations towards the end of the discharge now around 0.18–0.22 as H-mode dithering becomes more evident in the H_α traces. Such an H-mode can be sustained in steady state, but both n_{es} ($\sim 2 \times 10^{19}$ m^{-3}) and n_e^{lim} ($< 1 \times 10^{19}$ m^{-3}) are too low to be of interest for future divertor action on W7-AS.

2.3. Behavior for $P_{nbi} \sim 0.4$–1.2 MW

Certain trends in the examples above have general validity in the window around $\iota_a \sim 5/9$ where the H-mode is extant:

1. A threshold density $\bar{n}_e^{thr}$ must be exceeded to enter the H-mode,
2. $\bar{n}_e^{thr}$ is lower for ECRH discharges, and
3. $\bar{n}_e^{thr}$ increases with heating power.

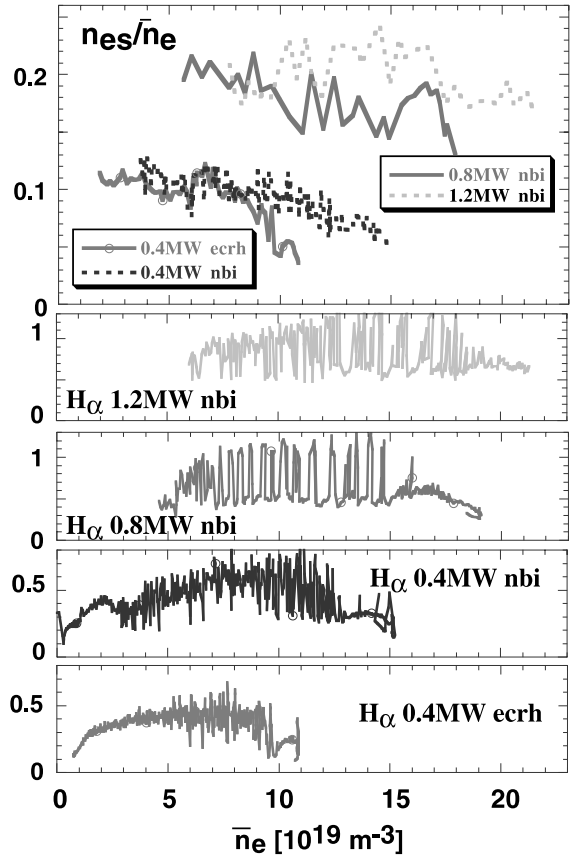

Fig. 3. $n_{es}/\bar{n}_e$ vs. $\bar{n}_e$ for three heating powers: P_{ecrh} (#47100) ~ P_{nbi} (#47108) ~ 0.4 MW; $P_{nbi} \sim 0.8$ MW (#47119); ~1.2 MW (#47120). Only occasional $n_{es}/\bar{n}_e$ points are evaluated, thus giving a dithering pattern other than H_α. Bottom – H_α traces at a limiter; $\iota_a = 0.55$.

These properties are quantified in a discharge series with $P_{ecrh} \sim 0.4$ MW and $P_{nbi} \sim 0.4$–1.2 MW. Fig. 3 exhibits $n_{es}/\bar{n}_e$ for all cases. The increase in $n_{es}/\bar{n}_e$ going from 0.4 to 0.8 MW is again evident; the change from 0.8 to 1.2 MW is not so large, but higher $\bar{n}_e$ pertain before H-mode dithering ceases and the H^* transition occurs. Thus, the path to conditions at the separatrix amenable to a high-recycling divertor is via higher heating powers, both to broaden the core density profiles in order to enhance $n_{es}/\bar{n}_e$ and to push entrance into the H-mode to higher $\bar{n}_e$. A data set (over $P_{nbi} \sim 0.4$–1.6 MW) including those of Fig. 3 yields: $\bar{n}_e^{thr}$ (10^{19} m^{-3}) ~ $7.7 P_{nbi}$ (MW) + 10, for $\iota_a \sim 558$ and the inherent radiation level of the series (indications are that $P_{sol} = P_{abs} - P_{rad}$ is the relevant quantity). See [1,3,4] for more discussion of H-mode details.

2.4. Achievement of high n_{es}

Fig. 4 illustrates salient features of two discharges tailored to maximize n_{es}, using $P_{nbi} \sim 2$ MW

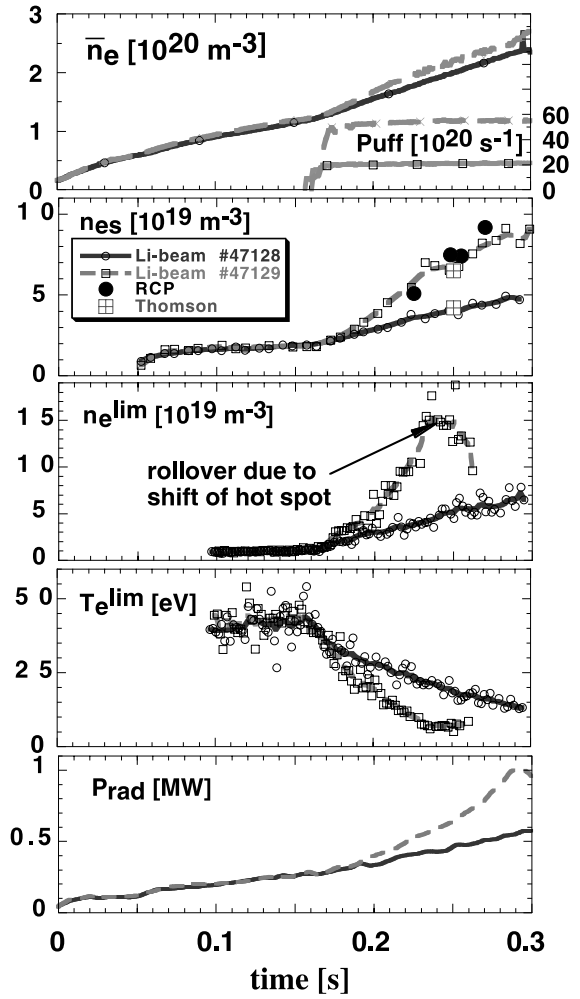

Fig. 4. Discharges with moderate and heavy gas puffing (respectively: solid lines – #47128, dashed lines – #47129): n_{es} from the Li beam (lines); RCP (dots) and edge Thomson (squares); n_e and T_e at lower limiter; $P_{nbi}^{abs} \sim 1.8$ MW. NBI fueling rate $\sim 2.5 \times 10^{20}$ s^{-1}; $\iota_a = 0.561$; $a_{eff} \sim 13.4$ cm.

($P_{abs} \sim 1.8$ MW) and hard density ramps. The shots differ in the puff rate, with the higher (#47129) being 20 times larger than that of NBI electron fueling. This stronger puff effects little difference in $\bar{n}_e$; however, the density profile broadens substantially as attested by the enhanced n_{es}. Maximum separatrix densities approaching 10^{20} m^{-3} are realized at $\bar{n}_e \sim 2.7 \times 10^{20}$ m^{-3}, whereby n_e^{lim} (lower limiter) peaks around 1.5×10^{20} m^{-3} and T_e^{lim} falls to below 10 eV. The rollover in n_e^{lim} suggests imminent plasma detachment from the limiter. Actually, it arises due to a shift of the hot spot at the limiter as it moves away from the Langmuir probe with increasing plasma beta. This is corroborated by a shift of the H_α profile seen by the CCD camera. Further, no concomitant decrease in the power to the limiter is seen by the IR camera at the I_{sat}^{lim} rollover – rather P_{lim}/P_{sol} remains rather constant throughout the discharge at $\sim$0.45–0.5. (About half the power goes to the walls for 5/9 configurations and inner limiters.)

n_{es} of Fig. 4 is independently determined from both the RCP and Thomson scattering. The Thomson system separatrix position is derived by assuming classical heat conduction along field lines to the target plate to derive the upstream temperature ($\sim$80 eV) compatible with the measured peak power flux at the limiter of $\sim$12 MW/m^2 at 0.25 s, and then taking the density at that point. The continuous traces of n_{es} originate from the Li beam, whose separatrix position is calibrated by averaging the results of Thomson and the RCP.

n_e^{lim} and I_{sat}^{lim} vs. n_{es} at the upper and lower limiters for both discharges are described by the characteristics: $n_e^{limup} \sim n_{es}^{1.38–1.40}$, $n_e^{limdown} \sim n_{es}^{1.88–1.92}$ and $I_{sat}^{limup} \sim n_{es}^{0.97–0.87}$, $I_{sat}^{limdown} \sim n_{es}^{1.43–1.36}$ with the two exponential values coming from #47128 and #47129, respectively. The dependencies are all weaker than expected from predictions of the 2-point model in the high-recycling region, e.g., $I_{sat}^{lim} \sim n_{es}^2$ and $n_e^{lim} \sim n_{es}^3$. Even though n_{es} and n_e^{lim} are large, it is not surprising that high-recycling characteristics do not pertain. The plasma–limiter interaction region is only a few cm^2 in size and is quite open, i.e., there are no baffling structures to promote neutral compression. With this in mind, the upstream–downstream electron pressures are compared in Fig. 5, whereby the upstream T_{es} is again derived from the 2-point model using the measured peak power deposition at the limiter as a function of time. $n_e T_e^{lim}$ for the upper limiter probe is about one-half the upstream pressure; the lower limiter probe has lower values both of which are consistent, within error, of a low-recycling regime over most of the range shown. Nonetheless, for $n_{es} T_{es} > 3 \times 10^{21}$ m^{-3} eV the curves tend to flatten, signifying entrance into moderate recycling qualitatively consistent with the cited I_{sat}^{lim} vs. n_{es} characteristics above.

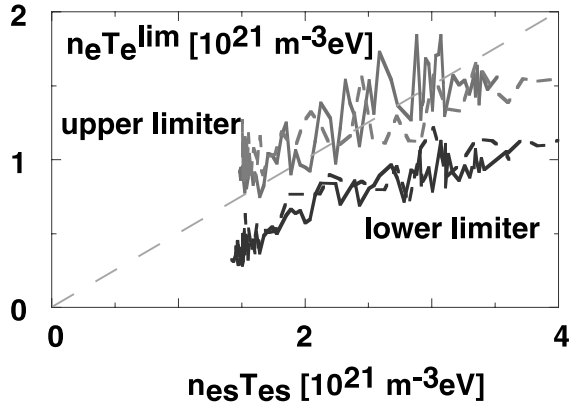

Fig. 5. $n_e T_e^{lim}$ vs. $n_{es} T_{es}$ for #47128 and #47129. The line $n_e T_e^{lim}/n_{es} T_e = 1/2$ is indicated.

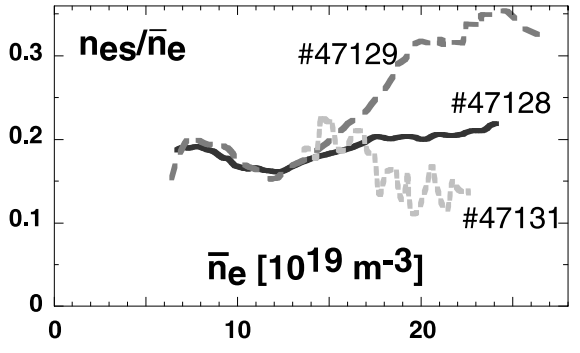

Fig. 6. $n_{es}/\bar{n}_e$ vs. $\bar{n}_e$ for #47128 and #47129 ($P_{nbi} \sim 2$ MW) and #47131 ($P_{nbi} \sim 1.2$ MW).

Fig. 6 depicts $n_{es}/\bar{n}_e$ vs. $\bar{n}_e$ for the two 2 MW discharges, and another at 1.2 MW for the same configuration. For moderate puffing (#47128), $n_{es}/\bar{n}_e \sim 0.2$; the heavy puff peaks at $n_{es}/\bar{n}_e \sim 0.35$, while the 1.2 MW exhibits L–H–L switching with corresponding fluctuations in n_{es} at levels about half that of #47128. Discharge #47129 displays n_{es}-values at a power P_{sol} for which EMC3 calculations have indicated detachment. Thus, within density ramps it should be feasible to probe this regime with divertor modules. Whether such high n_{es} can be maintained quasi-steady-state remains to be seen also from the standpoint of radiation. Presumably, P_{rad} will continue to climb in time even if the density profile could be held constant since the time constants for impurity profile equilibration are of the order of a second at higher densities [13]. A ratio $n_{es}/\bar{n}_e \sim 0.2$ seems more likely attainable on a longer time scale, implying $\bar{n}_e = 4 \times 10^{20}$ m^{-3} for $n_{es} = 8 \times 10^{19}$ m^{-3}. Using the expression for $\bar{n}_e^{DL}$ cited earlier [8] as a guide, P_{abs} must be greater than 2.2 MW just to avoid the density limit and still higher to sustain a useful plasma. These numbers are within operational limits, albeit at the extremes.

3. Summary

For an $\iota_a = 5/9$ configuration, in conjunction with the divertor modules being brought into operation on W7-AS, and $P_{sol} \sim 1$ MW the 3D EMC3 code predicts $n_{es} \sim 10^{20}$ m^{-3} is necessary to achieve detachment at the target plates. Results are presented for $n_{es}/\bar{n}_e$ over $\bar{n}_e \sim 0.2$–2.7×10^{20} m^{-3} and $P_{heat} \sim 0.4$–2 MW using 10 inner sector limiters, as a pre-study for the upcoming divertor phase. In principle, the density limit $\bar{n}_e^{DL}$, found to scale as $[P_{abs}/V_p]^{0.48} B_t^{0.54}$ for a variety of stellarators, should also define the upper end of obtainable separatrix densities at any given power. In practice, at lower powers the appearance of the ELM-free H mode H^*, or even 'L–H–L' switching modes, sets in at $\bar{n}_e < \bar{n}_e^{DL}$. At $P_{heat} \sim 0.4$ MW, the H^*-transition (around $\bar{n}_e \sim 10^{20}$ m^{-3}) results in $n_{es}/\bar{n}_e < 0.1$, and the improved confinement leads to radiation collapse of the core plasma on a confinement timescale. Further, at the $P_{heat} \sim 0.4$ MW level, the increase in τ_E with $\bar{n}_e$ is accompanied by a narrowing of the global density profile such that $n_{es}/\bar{n}_e$ changes over ~0.2–>0.1 before entering H^*. Generally, it is found for access to the H-mode there exists a threshold density $\bar{n}_e^{thr}$ which must be exceeded, and $\bar{n}_e^{thr}$ increases with heating power. (This behavior is in direct contrast to tokamaks where one must be below $\bar{n}_e^{thr}$ and above P_{heat}^{thr}, and not vice versa.) Evidence is that the edge ion temperature gradient becomes steeper with increasing $\bar{n}_e$, leading to higher radial electric fields which then cause $E \times B$ sheared flow and suppression of turbulence...to produce the H-mode [3].

For $P_{heat} \sim 0.8$–1.6 MW, $n_{es}/\bar{n}_e \sim 0.2$–0.15 with jumps in n_{es} of ~25% during the L–H–L switching phases. For $P_{nbi} \sim 2$ MW vestiges of the H-mode are largely suppressed; at $\bar{n}_e \sim 2.7 \times 10^{20}$ m^{-3}, attained by gas puffing in short density ramps, n_{es} approaching 10^{20} m^{-3} can be achieved, whereby within this fast ramp the density profiles are substantially broader than normal and $P_{rad}/P_{abs} \sim 50$–60%, yielding $P_{sol} < 1$ MW. Thus, at least transiently, it is shown that edge conditions necessary for predicted detachment with the divertor modules can be reached. This is important for validation efforts of EMC3 over a wide range of parameters. The extent to which quasi-steady-state detached scenarios can be studied must await experiment. With the advent of the divertor modules, recycling patterns will be altered – perhaps leading to a change in $n_{es}/\bar{n}_e$, or H-mode entrance conditions; and hopefully the core impurity level will be lower, permitting higher $\bar{n}_e$ before radiation collapse.

References

[1] K. McCormick, P. Grigull et al., Plasma Phys. Control. Fus. 41 (1999) B285.
[2] K. McCormick, P. Grigull, R. König et al., J. Plasma Fus. Res. Series 3 (2000) 169–175.
[3] P. Grigull, M. Hirsch et al., these Proceedings.
[4] P. Grigull et al., Europhysics Conf. Abs. 23J (1999) 1473.
[5] R.W.T. König, K. McCormick et al., these Proceedings.
[6] Y. Feng, F. Sardei, J. Kisslinger, Europhysics Conf. Abs. 23J (1999) 1465.
[7] Y. Feng, private communication.
[8] L. Giannone et al., Plasma Phys. Control. Fus. 42 (2000) 603.
[9] K. McCormick et al., in: Proceedings of the 12th International Stellarator Conference, Madison, 1999.
[10] J.P. Knauer et al., in: Proceedings as [9].
[11] D. Hildebrandt et al., in: Proceedings as [9].
[12] J. Sallander et al., in: Proceedings as [9].
[13] R. Burhenn et al., J. Plasma Fus. Res. Series 1 (1998) 255.